BACE2 processes PMEL to form the melanosome amyloid matrix in pigment cells

Leila Rochin[a,b], Ilse Hurbain[a,b,c], Lutgarde Serneels[d,e], Cecile Fort[a,b], Brenda Watt[f], Pascal Leblanc[g], Michael S. Marks[f], Bart De Strooper[d,e], Graça Raposo[a,b,c], and Guillaume van Niel[a,b,1]

[a]Institut Curie, Centre de Recherche and [b]Unité Mixte de Recherche 144, Centre National de la Recherche Scientifique, F-75248 Paris, France; [c]Cell and Tissue Imaging Facility, Infrastructures en Biologie Sante et Agronomie, 75248 Paris, France; [d]Center for Human Genetics and Leuven Institute for Neurodegenerative Diseases, University of Leuven, 3000 Leuven, Belgium; [e]VIB Center for the Biology of Disease, 3000 Leuven, Belgium; [f]Departments of Pathology and Laboratory Medicine and Physiology, University of Pennsylvania, Philadelphia, PA 19104; and [g]Laboratoire de Biologie Moléculaire de la Cellule, Centre National de la Recherche Scientifique, Unité Mixte de Recherche 5239, Ecole Normale Supérieure de Lyon, 60007 Lyon, France

Edited by Thomas C. Südhof, Stanford University School of Medicine, Stanford, CA, and approved May 15, 2013 (received for review December 13, 2012)

Amyloids are often associated with pathologic processes such as in Alzheimer's disease (AD), but can also underlie physiological processes such as pigmentation. Formation of pathological and functional amyloidogenic substrates can require precursor processing by proteases, as exemplified by the generation of Aβ peptide from amyloid precursor protein (APP) by beta-site APP cleaving enzyme (BACE)1 and γ-secretase. Proteolytic processing of the pigment cell-specific Melanocyte Protein (PMEL) is also required to form functional amyloid fibrils during melanogenesis, but the enzymes involved are incompletely characterized. Here we show that the BACE1 homologue BACE2 processes PMEL to generate functional amyloids. BACE2 is highly expressed in pigment cells and *Bace2*$^{-/-}$ but not *Bace1*$^{-/-}$ mice display coat color defects, implying a specific role for BACE2 during melanogenesis. By using biochemical and morphological analyses, combined with RNA silencing, pharmacologic inhibition, and BACE2 overexpression in a human melanocytic cell line, we show that BACE2 cleaves the integral membrane form of PMEL within the juxtamembrane domain, releasing the PMEL luminal domain into endosomal precursors for the formation of amyloid fibrils and downstream melanosome morphogenesis. These studies identify an amyloidogenic substrate of BACE2, reveal an important physiological role for BACE2 in pigmentation, and highlight analogies in the generation of PMEL-derived functional amyloids and APP-derived pathological amyloids.

Amyloids are insoluble protein or peptide aggregates with a cross β-sheet structure that are often associated with pathologic processes, such as the Aβ fibrils that correlate with neurodegeneration in Alzheimer's disease (AD). However, the amyloid fibrils can also be exploited for physiological processes. "Functional amyloids" have recently emerged in increasing numbers of physiological eukaryotic processes such as peptide hormone storage, long-term memory maintenance, and early steps of melanogenesis (1–3). The formation of physiological and pathological amyloid can require sequential proteolysis of a precursor to release amyloidogenic fragments. For example, cleavage of the amyloid precursor protein (APP) by the β-secretase, beta-site cleaving enzyme (BACE)1, and the γ-secretase complex (4) generates the amyloidogenic Aβ peptide in AD (5). Whether similar proteases control the formation of functional amyloid is not known. Neither BACE1 nor its close homologue BACE2, which has no role in APP processing during amyloidogenesis and few known substrates (6), is yet known to process other amyloidogenic proteins. Given the multiplicity of amyloidogenic substrates, we hypothesized that BACE proteases play a conserved role in functional amyloidogenesis.

As an excellent candidate for BACE-dependent amyloidogenesis, we focused on the physiological amyloids derived from processing of the pigment cell-specific protein Melanocyte Protein (PMEL) (also referred as Pmel17/silver/gp100) (7). PMEL was the first natural amyloid described in mammals and is thus far the best studied (8). PMEL is a type I transmembrane glycoprotein specifically expressed in pigment cells of the eye and skin. These cells synthesize melanin pigments within specialized lysosome-related organelles called melanosomes (9). As they are synthesized in melanosomes, melanins deposit on a sheet-like matrix of amyloid fibrils, the main components of which are proteolytic fragments of PMEL. The fibrils form within endosomal precursors of melanosomes through coordinated sorting events and enzymatic processing that culminate in a conformational change that drives physiological amyloid formation by luminal PMEL fragments (8). PMEL amyloidogenesis during the generation of early stage I and II melanosomes (10) underlies the ellipsoidal shape and striated ultrastructure of melanosomes, and facilitates melanocyte homeostasis likely by sequestering toxic intermediates in melanin synthesis as melanosomes mature (9, 11).

PMEL transition to the amyloid form requires proteolytic processing steps (12–14) that are reminiscent of APP processing but are incompletely characterized in pigment cells (Fig. S1*A*). They include (*i*) cleavage of the full-length transmembrane form of PMEL by a proprotein convertase (PC) into an amyloidogenic luminal Mα fragment and a disulfide-linked transmembrane domain-containing Mβ fragment (12), (*ii*) further cleavage of Mβ by an "endosomal" sheddase to release Mα linked to Mβ luminal domain (i.e., Mβ-N) from the transmembrane C-terminal fragment (CTF) and to allow Mα oligomerization to form amyloid fibrils (13, 14), (*iii*) further processing of Mα by unknown proteases into smaller fragments found in mature fibrils and fibrillar sheets (15, 16), and (*iv*) intramembrane proteolysis of the CTF by the γ-secretase complex (13, 14). The analogy between the processing of PMEL and APP led us to investigate the role of BACE secretases in PMEL processing and functional amyloid formation. By using in vivo, *in cellulo*, and in vitro assays, we demonstrate that BACE2, the major homologue of BACE expressed in pigment cells (17), is the sheddase required for the processing of the PMEL Mβ fragment and for subsequent functional amyloidogenesis. Our results extend the role of BACE secretases to functional amyloid biogenesis and define *BACE2* as an important pigmentation gene.

Results

***Bace2*$^{-/-}$ Mice Display Pigmentation Defect.** BACE1 and BACE2 mRNAs are both expressed in pigment cells, but BACE2 levels were 37-fold higher than BACE1 levels in retinal pigment

Author contributions: L.R. and G.v.N. designed research; L.R., I.H., L.S., C.F., and B.W. performed research; L.S., P.L., M.S.M., and B.D.S. contributed new reagents/analytic tools; L.R., B.D.S., and G.v.N. analyzed data; and L.R., M.S.M., B.D.S., G.R., and G.v.N. wrote the paper.

Conflict of interest statement: B.D.S. is consultant for several companies involved in the development of therapeutics for Alzheimer's disease.

This article is a PNAS Direct Submission.

[1]To whom correspondence should be addressed. E-mail: guillaume.van-niel@curie.fr.

This article contains supporting information online at www.pnas.org/lookup/suppl/doi:10.1073/pnas.1220748110/-/DCSupplemental.

epithelial cells (17), suggesting that BACE2 is the major BACE homologue in pigment cells. To address whether BACE secretases function during melanosome biogenesis, we first tested whether *Bace1*$^{-/-}$ and *Bace2*$^{-/-}$ mice exhibit coat color dilution, which reflects melanogenesis defects in mice (9). Compared with their WT littermates, previously generated *Bace2*$^{-/-}$ but not *Bace1*$^{-/-}$ mice (18) on a C57BL/6 background revealed a "silvery" coat color (Fig. 1*A*), similar to that of mice with *Pmel* mutations that impair PMEL accumulation in melanosomes (19). Coat color dilution in *Bace2*$^{-/-}$ mice might therefore reflect impaired melanosome morphogenesis caused by the inability to produce the PMEL amyloid fibril matrix in melanosomes (20). Consistently, morphological analysis by conventional EM of the retinal pigment epithelium (RPE) and skin melanocytes of *Bace2*$^{-/-}$ mice revealed abnormal melanosome morphology (Fig. 1*B* and Fig. S1*D*), particularly in the RPE, in which melanosomes form during a limited developmental period (21). The proportion of round melanosome profiles was significantly increased in *Bace2*$^{-/-}$ RPE (47% in *Bace2*$^{-/-}$ RPE vs. 29% in WT; Fig. 1*C*), but the number of melanosomes per cell in WT and *Bace2*$^{-/-}$ RPE was similar (Fig. S1*B*). In addition, skin melanocytes in *Bace2*$^{-/-}$ mice harbored unusual vacuolar compartments filled with dense unstructured aggregates, and were devoid of elongated fibril-containing premelanosomes (Fig. 1*D*). Although melanosomes in *Bace2*$^{-/-}$ melanocytes were densely pigmented, more than 80% of them harbored abnormal melanin deposits (Fig. S1*C*). These morphological features are similar to those of RPE and skin melanocytes in PMEL mutant *silver* and *Pmel*$^{-/-}$ mice (11, 20). Together, these observations demonstrate altered melanosome morphogenesis in the absence of BACE2, likely as a consequence of impaired PMEL amyloid fibril formation.

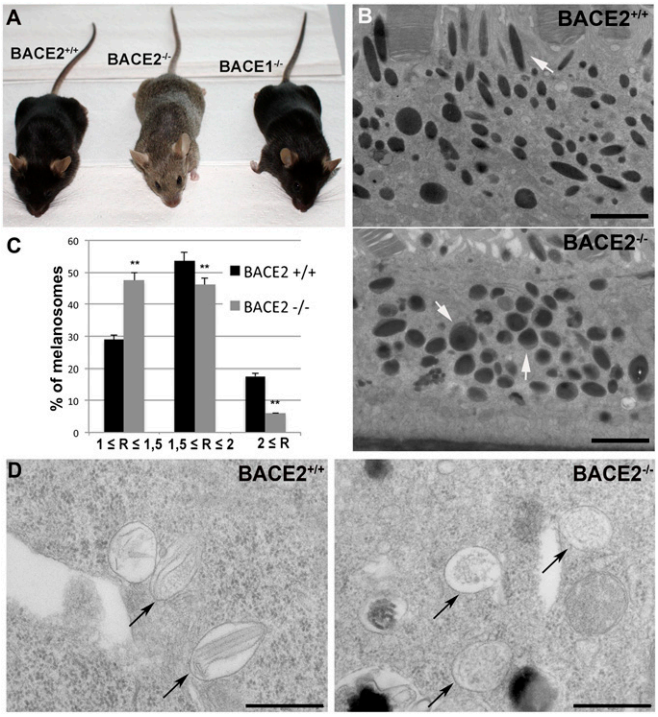

Fig. 1. Melanogenesis is impaired in *Bace2*$^{-/-}$ mice. (*A*) Coat color defect of *Bace2*$^{-/-}$ mice compared with their WT and *Bace1*$^{-/-}$ littermates. (*B*) EM analysis of epon-embedded RPE of WT and *Bace2*$^{-/-}$ mice. Note the presence of ellipsoidal-shaped melanosomes in WT mice and round-shaped melanosomes with heterogeneous melanin deposition in *Bace2*$^{-/-}$ mice (white arrows). (Scale bar: 1 μM.) (*C*) Ratio (marked as "R") between maximum width and length of an average of 150 melanosomes per condition. Melanosomes are significantly less elongated in *Bace2*$^{-/-}$ RPE (**$P \leq 0.01$). (*D*) Altered early-stage melanosome morphology in *Bace2*$^{-/-}$ skin melanocytes. Detail of epon-embedded dorsal skin sections of WT (*Bace2*$^{+/+}$) and *Bace2*$^{-/-}$ mice. Note the presence of stage II melanosomes containing amyloid fibrils in *Bace2*$^{+/+}$ mice and round vacuoles containing unstructured aggregates in *Bace2*$^{-/-}$ mice (black arrows). (Scale bar: 500 nm.)

BACE2 Depletion Inhibits Formation of PMEL-Derived Amyloid Fibrils in Cultured Melanocytic Cells. To further probe the requirement for BACE2 in PMEL-driven amyloidogenesis and melanosome morphogenesis, BACE2 was depleted by siRNA treatment in human pigmented MNT1 melanoma cells (see Fig. 4*A*), a faithful model for eumelanogenesis (22). Control and BACE2-depleted MNT1 cells were prepared by high-pressure freezing (HPF) and freeze substitution to preserve fibril structure, and thin sections were analyzed by EM (23) (Fig. 2*A*). Similar to observations in PMEL-deficient melanocytes (11, 20, 24), neither the number of stage IV melanized melanosomes nor the total melanin content was significantly reduced in MNT1 cells depleted for BACE2 (Figs. S2*A* and S3*A*). Moreover, the melanin-synthesizing enzyme tyrosinase-related protein 1 was localized appropriately to mature pigmented melanosomes in BACE2-depleted MNT1 cells (Fig. S3*B*), as reported in PMEL-deficient melanocytes (11, 20). However, BACE2 depletion resulted in a dramatic impairment of structured PMEL amyloid sheets, with a threefold decrease in the number of fibrillar stage II and III melanosomes and a sixfold increase in the number of round organelles containing unstructured aggregates (Fig. S2*A*); the latter abnormal organelles were very similar to those observed in *Bace2*$^{-/-}$ skin melanocytes (Fig. 1*D*). Because these organelles accumulated concomitantly with the loss of stage II and III melanosomes, they likely reflect a defect in early and not in late steps of melanogenesis.

To further assess how BACE2 depletion impairs amyloidogenesis, we generated 3D tomographic reconstructions from single tilt tomographic analyses of thick sections of control and BACE2-depleted MNT1 cells prepared by HPF and freeze substitution. In control MNT1 cells, PMEL fibrils begin to form in stage I premelanosomes from intraluminal vesicles and organize into parallel sheets in stage II melanosomes (23). BACE2 depletion strongly impaired the organization of fibrils into parallel sheets, leading to accumulation of aggregates of small fibrils (Fig. 2*B*). These dense aggregates contain PMEL, as indicated by immunogold labeling on ultrathin cryosections of BACE2-depleted cells using an antibody to the PMEL luminal domain (Fig. 2*C*). Taken together, these observations support a requirement for BACE2 in the maturation of PMEL fibrils and their assembly into sheets.

BACE2 Closely Apposes with PMEL in Melanosomes. Organelles with irregular electron-dense deposits are observed in pigment cells with impaired amyloid formation as a result of a loss of PMEL expression (in *Pmel*$^{-/-}$ mice) (11) or impaired endosomal sorting (14, 20) or processing (12) of PMEL. However, immunofluorescence microscopy (IFM) of BACE2-depleted MNT1 cells using an antibody to the PMEL luminal domain revealed punctate labeling, confirming that PMEL expression and trafficking to post-Golgi compartments, per se, were not impaired (Fig. S3*C*). By standard EM and immuno-EM analyses, the formation of multivesicular bodies and the sorting of PMEL to intraluminal vesicles also proceeded normally in the absence of functional BACE2 (Fig. 2*C*, *Inset*, and Fig. S2*A*). Given the role of the BACE2 homologue BACE1 in APP processing to the amyloidogenic Aβ, we reasoned that BACE2 might function in processing PMEL to its amyloidogenic state. If this were true, BACE2 would be expected to localize in melanocytes to compartments in which PMEL processing occurs. By IFM, endogenous BACE2 could not be detected (even though it was detected by immunoblotting; Fig. 4*A*), but overexpressed BACE2 localized to

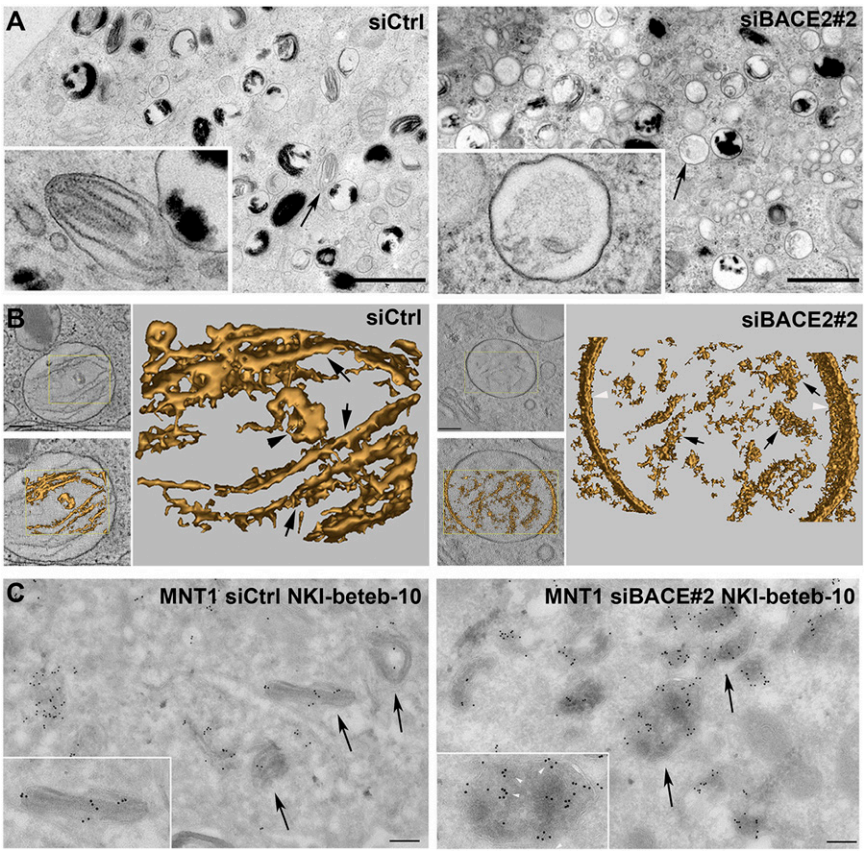

Fig. 2. BACE2 depletion affects PMEL-derived amyloidogenesis. (*A*) EM analyses of HPF/freeze substituted MNT1 cells treated with control (siCtrl) or BACE2 (siBACE2) siRNA. Black arrows indicate a stage II melanosome containing PMEL amyloid fibrils in control cells and a vacuole containing unstructured aggregates in BACE2-depleted cells; a magnified view is also shown (*Inset*). (Scale bar: 500 nm.) Fig. S2*A* provides quantification of endosomal/melanosomal compartments in siCtrl and siBACE2 cells. (*B*) Three-dimensional single tilt electron tomographic reconstructions were performed on thick sections of MNT1 cells treated with control or BACE2 siRNA. In control cells, black arrows indicate PMEL fibrils and the black arrowhead indicates intraluminal vesicles in a stage II melanosome. In BACE2-depleted cells, black arrows point to unstructured aggregates and white arrowheads indicate limiting membrane of a vacuolar compartment (Scale bar: 150 nm.) Fig. S2*B* shows tilt series and tomographic reconstruction. (*C*) EM analysis of ultrathin cryosections of MNT1 cells treated with control or BACE2 siRNA and Immunogold labeled for PMEL luminal domain [NKI beteb; protein-A gold 10-nm diameter (Pag 10)]. Note the presence of PMEL luminal labeling in fibrillar structures in control cells and in unstructured aggregates in BACE2-depleted cells (black arrows). Corresponding structures are also shown magnified (*Inset*); note the association of PMEL with intraluminal vesicles (white arrowheads) in BACE2-depleted cells. (Scale bar: 200 nm.)

puncta that partially overlapped with labeling for the PMEL luminal domain (Fig. 3*A*). To better appreciate the compartments in which PMEL and BACE2 overlapped, we performed an in situ proximity ligation assay (PLA) (25), in which fluorescent puncta are detected only when two proteins are in close proximity (<40 nm). By using antibodies directed against BACE2 and the PMEL luminal domain, we detected punctate PLA fluorescence in MNT1 cells expressing exogenous BACE2 but not in cells expressing an empty vector (Fig. 3*B*). The puncta were substantially less numerous than those labeled by IFM for BACE2 or PMEL alone. This indicates that PMEL and BACE2 are in close proximity within a subset of punctate compartments. By using immunolabeling and EM analysis of cryosections of MNT1 cells overexpressing BACE2, the compartments in which BACE2 colocalized with PMEL and CD63 [enriched in melanosomes (14)] were identified as stage I and II melanosomes (Fig. 3*C*). Thus, BACE2 is present in a subset of PMEL-containing melanosomes, likely reflecting involvement of BACE2 in PMEL processing at an early stage of melanosome biogenesis.

BACE2 Releases PMEL Luminal Domain to Generate Amyloidogenic Mα Fragment. To determine whether BACE2 functions in PMEL processing, we analyzed the effect of siRNA-mediated BACE2 depletion on the production of the different cleaved forms of PMEL in MNT1 cells. In control cells, PMEL is cleaved sequentially by a series of proteases to distinct fragments that can be detected by immunoblotting (Fig S1*A*). The efficiency of each cleavage can be deduced by immunoblotting by using the αPmel-C antibody; in control cells, this antibody detected the immature core-glycosylated P1 form (90 kDa), the Mβ (28 kDa) product of PC cleaved full-length PMEL, and the CTF (10 kDa) product of the cleavage of Mβ (Fig. 4*A* and Fig. S1*A*). By using a metabolic pulse/chase analysis of MNT1 cells and immunoprecipitation of PMEL fragments with αPmel-C antibody, we observed that treatment with the γ-secretase inhibitor N-[N-(3,5-Difluorophenacetyl)-L-alanyl]-S-phenylglycine t-butyl ester (DAPT) delays the accumulation of the CTF relative to Mβ (Fig. S4*A*); this indicates that PC cleavage precedes sheddase cleavage.

In cells treated with siBACE2#2 (which depletes BACE2 by 75%), the steady-state level of Mβ was increased nearly threefold whereas the level of CTF was decreased by 60%, indicating a defect in sheddase cleavage of Mβ (Fig. 4*A*). Similar results were observed with the use of three other BACE2 siRNAs (Fig. S4*B*). When they have been released from the membrane in control cells, Mα fragments assemble into Triton X-100 (TX)-insoluble fibrils (12) and undergo further proteolytic processing to smaller fragments (detected by antibodies HMB45 and I51) (16, 26, 27) (Fig. S1*A*). The level of I51-detectable fragments was not affected by BACE2 depletion, but levels of HMB45-reactive fragments were reduced by 70% (Fig. 4*B*). The TX-insoluble fractions were also aberrantly enriched in Mβ (detected by αPmel-C) and in misprocessed and aggregated forms of Mα (detected by αPmel-N), but not in an unrelated membrane marker (transferrin receptor; Fig. 4*B*). These data indicate that normal cleavage and polymerization of PMEL is impaired by BACE2 depletion.

To test whether BACE2 is also required for PMEL cleavage in vivo, we probed cryosections of developing RPE cells from neonatal WT and *Bace2*$^{-/-}$ mice by PLA (28) by using HMB45 and αPmel-C as primary antibodies. We reasoned that Mβ cleavage should separate the luminal HMB45 epitope on Mα from the cytoplasmic αPmel-C epitope on the CTF, reducing the PLA signal. Consistent with this prediction, very little PLA signal was observed in RPE of WT mice, but a consistent PLA signal was observed in RPE of *Bace2*$^{-/-}$ mice (Fig. 4*C* and Fig. S4*C*). The increase of fluorescent puncta in *Bace2*$^{-/-}$ mice supports the view that full-length PMEL accumulates in *Bace2*$^{-/-}$ RPE cells as it

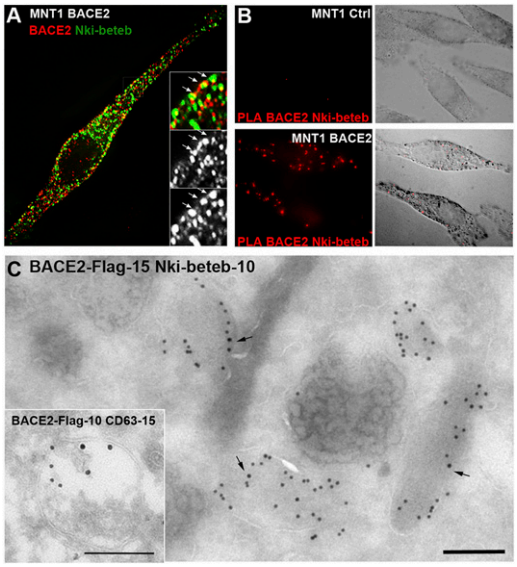

Fig. 3. BACE2 partially colocalizes and interacts with PMEL. (*A*) IFM analysis of MNT1 cells transfected with a BACE2-Flag construct, labeled for PMEL (NKI beteb) and BACE2-Flag. Insets and white arrows show examples of partial colocalization of BACE2 with PMEL. (*B*) PLA signals between BACE2-Flag and PMEL (NKI beteb) in MNT1 cells transfected with BACE2-Flag or an empty vector as a control (Ctrl) observed by IFM (*Left*) and merged with a bright-field image (*Right*). (*C*) EM analysis of ultrathin cryosections of MNT1 cells transfected with BACE2-Flag construct and Immunogold-labeled for PMEL luminal domain (NKI beteb; PAG 10) and BACE2-Flag (PAG 15; main image) or for BACE2-Flag (PAG 10) and CD63 (PAG 15; *Inset*). Black arrows indicate BACE2-Flag labeling in melanosomes. (Scale bar: 200 nm.)

does in BACE2-depleted MNT1 cells. By using HMB45 and αPmel-C to label ultrathin cryosections of the RPE, we also observed that both domains of PMEL recognized by these antibodies localize to unstructured melanosomes in *Bace2*$^{-/-}$ but not in *Bace2*$^{+/+}$ RPE (Fig. S4*D*). These data confirm the accumulation of full-length PMEL in the absence of BACE2 in vivo.

To complement analyses of BACE2 depletion, we assessed the effects of BACE2 overexpression on PMEL processing in MNT1 cells. BACE2 overexpression resulted in depletion of Mβ and accumulation of CTF at steady state (Fig. 4*D*). Similarly, overexpression of BACE2 in BACE2-depleted MNT1 cells also rescued the production of CTF (Fig. S4*E*). To determine whether BACE2 cleaves PMEL directly, we performed in vitro processing assays by using recombinant proteins. Treatment of full-length recombinant PMEL with recombinant BACE2 for 10 min resulted in the generation of a PMEL fragment that comigrates with PMEL CTF and that is recognized by αPmel-C antibody (Fig. 4*E*). Similar results were obtained when BACE2 was added to unprocessed PMEL that was immunoprecipitated from MNT1 cell lysates by using an antibody (αPmel-I) that binds only to preprocessed PMEL isoforms (26) (Fig. 4*E*). Using similar conditions, APP but not PMEL was cleaved by BACE1 (Fig. S4*F*).

Finally, to confirm that the impaired PMEL cleavage in BACE2-depleted cells reflected a loss of BACE2 proteolytic activity, we treated MNT1 cells with β-secretase inhibitor IV. At high concentrations, this inhibitor acts on BACE1 and BACE2, but, at low concentrations, it blocks only BACE1 (29). Treatment of MNT1 cells with the high concentration of β-secretase inhibitor IV, but not the low concentration, resulted in increased levels (45%) of Mβ at steady state compared with cells treated with a vehicle control (Fig. S4*G*). Addition of high concentrations of β-secretase inhibitor IV also inhibited PMEL CTF production in our in vitro processing assays (Fig. 4*E*). This supports the notion that the proteolytic activity of BACE2, but not of BACE1, is required for Mβ cleavage.

A previous study implicated the α-secretases a disintegrin and metalloproteinase (ADAM)10 and ADAM17 as necessary for Mβ cleavage in PMEL-expressing transfected HeLa cells (13). However, in MNT1 cells, ADAM10 did not show intracellular colocalization with PMEL (Fig. S4*H*), and treatment with siRNA to ADAM10 (Fig. S4*I*) or with inhibitors of α-secretases (Fig. S4*G*) did not consistently affect PMEL cleavage, causing only a moderate reduction of intracellular HMB45-reactive fragments. Moreover, CTF of PMEL in MNT1 cells and PMEL-expressing transfected HeLa cells did not display similar molecular weights (Fig. S4*J*), and production of the CTF in PMEL-expressing transfected HeLa cells was not sensitive to BACE2 depletion (Fig. S4*K*). These observations demonstrate that PMEL-Mβ follows distinct processing in PMEL-expressing transfected HeLa cells and in pigment cells.

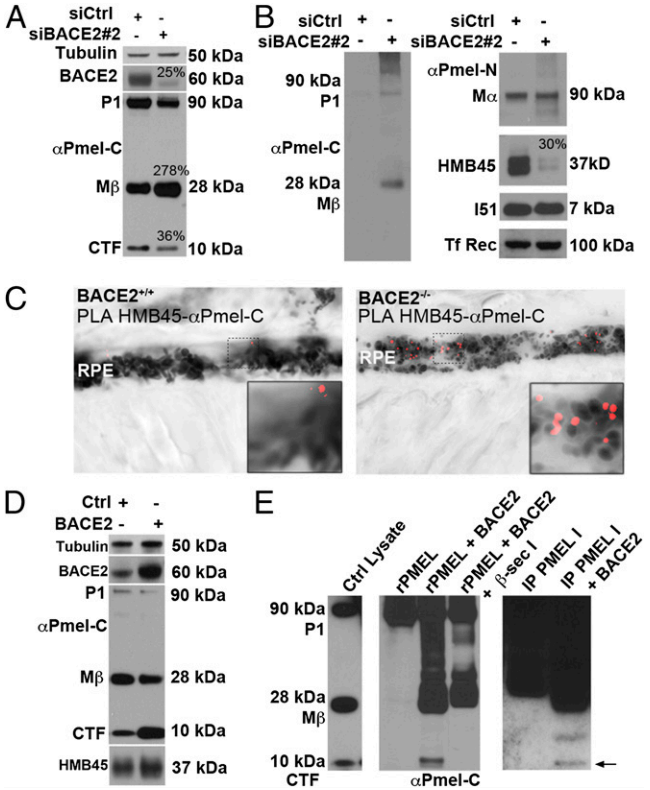

Fig. 4. BACE2 cleaves PMEL-Mβ. (*A*) TX-soluble lysates of MNT1 cells treated with control or BACE2 siRNA were analyzed by immunoblotting by using antibodies against the PMEL C terminus (αPMEL-C), BACE2, and tubulin as a loading control. BACE2 knock-down increases the relative abundance of Mβ and decreases the abundance of the CTF. (*B*) TX-insoluble material from the same cells was analyzed by using αPMEL-C, αPMEL-N (which recognizes Mα), HMB45 and I51 (which recognize distinct fragments of Mα associated with PMEL fibrils), and transferrin receptor. Note the accumulation of Mβ and uncleaved Mα and a loss of HMB45-reactive fragments upon depletion of BACE2. (*C*) Merged image illustrating PLA signal quantified in Fig. S4*C* and the corresponding bright field showing melanosomes with PLA signal. (*D*) Lysates of MNT1 cells transfected with BACE2 or an empty vector (Ctrl) were analyzed by immunoblotting as in *A* and *B*. Note the decrease of Mβ and the increase of CTF in the BACE2-overexpressing cells. (*E*) PMEL cleavage by BACE2 in vitro. A soluble recombinant PMEL (rPMEL) or the uncleaved form of PMEL immunoprecipitated from TX-soluble lysates of MNT1 cells with αPmel-I antibody (IP PMEL I) was incubated in the absence or presence of soluble recombinant BACE2 with or without β-secretase inhibitor (β-sec I). The products of the reactions were analyzed by immunoblotting using αPMEL-C and compared with signals obtained from untreated MNT1 cell lysate (Ctrl lysate). BACE2 addition to either source of PMEL leads to the production of a fragment that migrates similarly to the CTF (black arrow); addition of β-secretase inhibitor prevents cleavage.

Altogether, these data demonstrate that, in pigment cells, BACE2 functions as the endosomal sheddase that cleaves PMEL-Mβ and releases the amyloidogenic PMEL luminal domain containing Mα and Mβ-N fragments that is required for subsequent processing of fibrillogenic Mα.

Discussion

Our results define a physiological and amyloidogenic substrate for BACE2 in pigment cells. Contrary to BACE1, BACE2 has no known role in Aβ generation or the etiology of AD (30), and to date has been implicated in the degradation of Aβ (31) and in the maintenance of pancreatic β-cell function and mass through the cleavage of transmembrane protein 27 (TMEM27) (32). Very recently, loss of BACE2 activity in zebrafish was shown to modestly influence pigmentation by an apparent alteration in melanophore migration, whereas loss of BACE1 activity had no apparent effect on pigmentation (33), consistent with the absence of hypopigmentation defect in *Bace1*$^{-/-}$ mice. Although a migration defect could account for the coat color dilution observed in *Bace2*$^{-/-}$ mice, we propose that hypopigmentation also reflects melanocyte mortality caused by leakage of melanin and cytotoxic intermediates, as has been proposed for PMEL-deficient *silver* and *Pmel*$^{-/-}$ mice (11, 34).

Our work and other studies (13, 14) reveal similarities in the processing of functional and pathogenic amyloid substrates. However, we could not demonstrate a role for BACE1 in PMEL cleavage. The molecular basis for BACE subtype specificity in PMEL cleavage is not totally clear, but likely in part reflects the differential expression (17) and subcellular compartmentalization of BACE1 and BACE2 in pigment cells. Although substrate recognition also likely differs between BACE1 and BACE2, BACE2 has no known consensus recognition site (35), and the sheddase cleavage site for PMEL that is likely targeted by BACE2 in MNT1 cells (13) shares only a single leucine with other known BACE2 substrates like TMEM27 (32), or seizure 6-like protein (35).

PMEL sheddase activity upon ectopic expression in HeLa cells was previously ascribed to ADAM10 (13). Although ADAM10 is expressed in melanocytes, its inhibition and/or depletion did not significantly alter PMEL processing in MNT1 cells. Similar differences between PMEL-transfected HeLa and melanocytic cells have been reported for the PC mediated cleavage of full-length PMEL (20, 36). We speculate that this difference results from the distinct localization of ADAM10 in pigment cells and HeLa cells caused by cell type-specific regulators (37) and limitation of the proteolytic activity of ADAM10 to the plasma membrane of pigment cells and not in endosomes (38). We therefore conclude that ADAM10 does not function in the intracellular formation of PMEL amyloid in pigment cells. However, ADAM10 might participate in PMEL shedding from the plasma membrane (36) as reported previously (13) and suggested by the persistence of low levels of the PMEL-derived CTF in BACE2-depleted cells.

Our work defines BACE2 as a tissue-specific protease and defines *BACE2* as a pigmentation gene. Although numerous genetic loci in which mutations affect pigmentation have been identified (39), genes required for early steps of melanogenesis might have been missed because their disruption causes only minor coat color alterations (11). Moreover, our demonstration here of the generation of functional PMEL amyloid by BACE2 highlights analogies with the generation of pathogenic amyloid from APP by the highly homologous BACE1. Our work therefore strengthens the model of physiological formation of PMEL-derived amyloids as a template to investigate the mechanisms involved in the generation of pathological amyloid during AD. For PMEL, regulated cleavage by BACE2 within melanosome precursors likely serves as a mechanism to accurately time and compartmentalize amyloid formation within melanocytes. This regulation likely contributes to the lack of toxicity of the amyloid fibrils and of the intermediates in fibril formation toward cellular components that might be present in earlier compartments (7).

Materials and Methods

Mice. Dorsal skin and eyes from *Bace1*$^{-/-}$, *Bace2*$^{-/-}$ and WT mice (3 mo of age for Fig. 1 *B* and *C* and Fig. S1 *B* and *C*; 5 d of age for Figs. 1*D* and 4*C* and Fig. S4 *C* and *D*) ($n = 4$) on the C57BL/6J background (18) were dissected and fixed. Dorsal skin was fixed by immersion in modified Karnovsky's fixative (2% paraformaldehyde, 2% (wt/vol) glutaraldehyde, 0.06% $CaCl_2$, 0.1 M cacodylate buffer, pH 7.3) at 4 °C. Eyes were dissected after transcardial perfusion with ice-cold PBS solution followed with 4% (wt/vol) paraformaldehyde and 2% (wt/vol) glutaraldehyde in PBS solution, and postfixed by immersion in 0.1 M cacodylate buffer, pH 7.2, containing 2.5% (wt/vol) glutaraldehyde. Mice were housed under specific pathogen-free conditions and were used in accordance with the University of Leuven Animal Ethics Committee.

Cell Culture, Drug Treatment, Transfection, and siRNA Depletion. HeLa cells expressing PMEL and human melanocytic MNT1 cells were maintained as previously described (10, 22). Cells were treated for 24 h with α-secretase inhibitor tumor necrosis factor-α protease inhibitor-2 (TAPI II) (Enzo Life Sciences), DAPT (Sigma Aldrich), or β-secretase inhibitor IV (Calbiochem). Cells were subjected to one round of siRNA transfection with siRNA duplex oligonucleotides as reported, and collected after 72 h (24). MNT1 cells were transfected with plasmid constructs by using Lipofectamine 2000 (Invitrogen) following the manufacturer's recommendations, and collected after 48 h. For rescue experiment, cells were subjected to two rounds of siRNA transfection and transfected with plasmid constructs for BACE2 after 72 h and collected after 24 h. BACE2 constructs were generated and provided by B.d.S. (40). APP cDNA was a gift of Jean-Baptiste Brault (Unité mixte de Recherche 144, CNRS, Paris, France). siRNA sequences as well as antibodies list are detailed in *SI Materials and Methods*.

Immunoprecipitation. TX-soluble material from MNT1 and HeLa cells was obtained as previously described (10) and precleared for 30 min by addition of 50 μL protein G–agarose beads (Invitrogen) and for 30 min by addition of 50 μL protein G–agarose beads coated with irrelevant rabbit antibody (Dako). Proteins were then immunoprecipitated by adding 50 μL protein G–agarose beads coated with αPmel-I in MNT1 lysates and antibody specific for APP luminal domain antibody in HeLa cells lysate. After 2 h at 4 °C under constant agitation, beads were washed five times in lysis buffer. The immunoprecipitates were subjected to in vitro cleavage as described below in In Vitro Cleavage.

Western Blot. TX-soluble and insoluble material from MNT1 cells was obtained as previously described (10) and analyzed by Western blot as described previously (14). Signal intensities were quantified with ImageJ software.

In Vitro Cleavage. PMEL (0.40 μg), SILV human recombinant protein P01 (Abnova), or immunoprecipitates against PMEL or APP were incubated with 1.6 μg of recombinant BACE2 (Enzo Life Sciences) or with 2 μg of recombinant BACE1 (Enzo Life Sciences) in assay buffer (Enzo Life Sciences). As a control, no recombinant BACE2 was added or β-secretase inhibitor IV was added to the PMEL/BACE2 mixture. After 10 min, the reaction mixture was withdrawn, incubated in sample buffer, and analyzed by SDS/PAGE.

IFM. Untreated, drug-treated, or transfected MNT1 cells were grown on coverslips at 70% confluence and treated for IFM as previously described (14) and examined on a Leica DM-RXA2 3D deconvolution microscope equipped with a piezo *z* drive (Physik Instrument) and a 100× 1.4 NA PL-APO objective lens. Images are maximum-intensity *z* projections of 3D image stacks (except Fig. S4*H*, which shows a single deconvolved layer) acquired every 0.2 μm using Metamorph software (MDS Analytical Technologies) and a Coolsnap HQ cooled CCD camera (Photometrics).

PLA. BACE2-transfected MNT1 cells were fixed for 15 min in 4% paraformaldehyde/PBS solution at room temperature. Whole eyes of 5-d-old WT and *Bace2*$^{-/-}$ mice were dissected and fixed in 4% (wt/vol) PFA/PBS solution for 2 h, washed for 10 min in PBS solution, and cryoprotected in 30% (wt/vol) sucrose for 24 h before being frozen in optimum cutting temperature compound (TBS tissue freezing medium), cryosectioned (8-μm sections), and collected on Superfrost Plus glasses (Menzel-Gläser). Fixed cells and cryosections were washed in PBS solution and blocked and permeabilized

during 30 min with PBS solution/0.1% saponin/BSA 0.2%. After incubation with primary antibodies, their proximity was assayed by using the Duolink II PLA Probes and detection kit (Olink Bioscience) according to manufacturer instructions. Images were acquired as described earlier for IFM and compared with the corresponding bright-field 8-bit image. Cell counter was delineated by using the polygon selection tool in ImageJ software, and the number of dots corresponding to the PLA signal was determined by using the colocalization plug-in (Pierre Bourdoncle, Cochin Institut, Paris, France) and then object counter 3D (i.e., counting number of 3D objects in *z*). The mean value of PLA signal was determined on 18 cells.

EM. For conventional EM analysis of RPE sections and dorsal skin sections, tissues from *Bace2*$^{-/-}$ mice and WT mice were processed for epon embedding and ultrathin sections and then contrasted with uranyl acetate and lead citrate as described previously (21). For ultrathin cryosectioning and Immunogold labeling, BACE2 MNT1-depleted cells, BACE2-Flag transfected MNT1 cells, and tissue blocks from the eyes were processed for ultracryomicrotomy and single or double Immunogold labeling using PAG10 and PAG15 as reported (22). All samples were analyzed by using a FEI CM120 electron microscope (FEI Company), and digital acquisitions were made with a numeric camera (Keen View; Soft Imaging System).

Electron Tomography. MNT1 cells grown on carbonated sapphire discs were high-pressure frozen and processed as described previously (23, 41). Tomographic acquisitions were made on 300-nm-thick sections. Tilt series (angular range from –65° to +65° with 1° increments) were recorded by using Xplore3D (FEI) or TEMography (JEOL) on 200-kV transmission electron microscopes (Tecnai 20 LaB6, FEI; or JEM 2200FS equipped with an Ω-filter; JEOL). A 10-eV energy window was used to record *Z*-loss filtered images with the JEOL electron microscope. Images (1,024 × 1,024 pixels) were recorded using a CCD camera (Temcam F214; TVIPS; or Ultrascan 894; Gatan). Tilt series alignment and weighted back-projection reconstruction were performed by using eTomo (IMOD) software (42). PAG 10 at the surface of the sections were used as fiducial markers. Reconstructed structures were computationally identified with the isosurface selection tool in IMOD (42).

Image Analysis and Quantification. Melanosome stages were defined by morphology (22, 43). Quantification of the length and width of melanosomes was determined by using iTEM software (Soft Imaging System).

ACKNOWLEDGMENTS. We thank Siska Deforce, who first drew our attention to the silver coat color of *Bace2*$^{-/-}$ mice; C. Delevoye, Tina Ho, Gwendoline Gros, Gaëlle Boncompain, Eric Rubinstein, Francesca Giordano, Guillaume Montagnac, and Jean-Baptiste Brault for technical help, insightful discussions, and critical reading of the manuscript; and V. Fraisier and L. Sengmanivong [The BioImaging Cell and Tissue Core Facility of the Institut Curie (PICT-IBiSA), Institut Curie; Nikon Imaging Center] for assistance with deconvolution microscopy. This work was supported by Institut Curie, Centre National de la Recherche Scientifique, Fondation ARC pour la Recherche sur le Cancer Grant SL220100601359 (to G.R.), National Institutes of Health Grant R01 AR048155 (to M.S.M.), Fund for Scientific Research Flanders, Katholieke Universiteit Leuven, a Methusalem Grant from Katholieke Universiteit Leuven and the Flemish government, Stichting Alzheimer Onderzoek/Fondation pour la Recherche sur la Maladie d'Alzheimer (SAO/FRMA), and Interuniversity Attraction Poles Program P7/16 of the Belgian Federal Science Policy Office. B.D.S. is the Arthur Bax and Anna Vanluffelen Chair for Alzheimer's disease.

1. Fowler DM, et al. (2006) Functional amyloid formation within mammalian tissue. *PLoS Biol* 4(1):e6.
2. Maji SK, et al. (2009) Functional amyloids as natural storage of peptide hormones in pituitary secretory granules. *Science* 325(5938):328–332.
3. Majumdar A, et al. (2012) Critical role of amyloid-like oligomers of Drosophila Orb2 in the persistence of memory. *Cell* 148(3):515–529.
4. De Strooper B (2010) Proteases and proteolysis in Alzheimer disease: A multifactorial view on the disease process. *Physiol Rev* 90(2):465–494.
5. De Strooper B, Vassar R, Golde T (2010) The secretases: Enzymes with therapeutic potential in Alzheimer disease. *Nat Rev Neurol* 6(2):99–107.
6. Fluhrer R, et al. (2002) A non-amyloidogenic function of BACE-2 in the secretory pathway. *J Neurochem* 81(5):1011–1020.
7. Watt B, Raposo G, Marks MS (2010) Pmel17: An amyloid determinant of organelle structure. *Functional Amyloid Aggregation*, eds Rigacci S, Bucciantini M (Trivandrum, Kerala, India), pp 89–113.
8. Watt B, van Niel G, Raposo G, Marks MS (2013) Pmel: A pigment cell-specific model for functional amyloid formation. *Pigment Cell Melanoma Res* 26(3):300–315.
9. Raposo G, Marks MS (2007) Melanosomes—dark organelles enlighten endosomal membrane transport. *Nat Rev Mol Cell Biol* 8(10):786–797.
10. Berson JF, Harper DC, Tenza D, Raposo G, Marks MS (2001) Pmel17 initiates premelanosome morphogenesis within multivesicular bodies. *Mol Biol Cell* 12(11):3451–3464.
11. Hellström AR, et al. (2011) Inactivation of Pmel alters melanosome shape but has only a subtle effect on visible pigmentation. *PLoS Genet* 7(9):e1002285.
12. Berson JF, et al. (2003) Proprotein convertase cleavage liberates a fibrillogenic fragment of a resident glycoprotein to initiate melanosome biogenesis. *J Cell Biol* 161(3):521–533.
13. Kummer MP, et al. (2009) Formation of Pmel17 amyloid is regulated by juxtamembrane metalloproteinase cleavage, and the resulting C-terminal fragment is a substrate for gamma-secretase. *J Biol Chem* 284(4):2296–2306.
14. van Niel G, et al. (2011) The tetraspanin CD63 regulates ESCRT-independent and -dependent endosomal sorting during melanogenesis. *Dev Cell* 21(4):708–721.
15. Kushimoto T, et al. (2001) A model for melanosome biogenesis based on the purification and analysis of early melanosomes. *Proc Natl Acad Sci USA* 98(19):10698–10703.
16. Watt B, et al. (2009) N-terminal domains elicit formation of functional Pmel17 amyloid fibrils. *J Biol Chem* 284(51):35543–35555.
17. Wang J, Ohno-Matsui K, Morita I (2012) Elevated amyloid β production in senescent retinal pigment epithelium, a possible mechanism of subretinal deposition of amyloid β in age-related macular degeneration. *Biochem Biophys Res Commun* 423(1):73–78.
18. Dominguez D, et al. (2005) Phenotypic and biochemical analyses of BACE1- and BACE2-deficient mice. *J Biol Chem* 280(35):30797–30806.
19. Dunn LC, Thigpen LW (1930) The silver mouse: A recessive color variation. *J Hered* 21(12):495–498.
20. Theos AC, et al. (2006) Dual loss of ER export and endocytic signals with altered melanosome morphology in the silver mutation of Pmel17. *Mol Biol Cell* 17(8):3598–3612.
21. Lopes VS, Wasmeier C, Seabra MC, Futter CE (2007) Melanosome maturation defect in Rab38-deficient retinal pigment epithelium results in instability of immature melanosomes during transient melanogenesis. *Mol Biol Cell* 18(10):3914–3927.
22. Raposo G, Tenza D, Murphy DM, Berson JF, Marks MS (2001) Distinct protein sorting and localization to premelanosomes, melanosomes, and lysosomes in pigmented melanocytic cells. *J Cell Biol* 152(4):809–824.
23. Hurbain I, et al. (2008) Electron tomography of early melanosomes: Implications for melanogenesis and the generation of fibrillar amyloid sheets. *Proc Natl Acad Sci USA* 105(50):19726–19731.
24. Theos AC, et al. (2006) A lumenal domain-dependent pathway for sorting to intralumenal vesicles of multivesicular endosomes involved in organelle morphogenesis. *Dev Cell* 10(3):343–354.
25. Teranishi Y, et al. (2012) Erlin-2 is associated with active gamma-secretase in brain and affects amyloid beta-peptide production. *Biochem Biophys Res Commun* 424(3):476–481.
26. Harper DC, et al. (2008) Premelanosome amyloid-like fibrils are composed of only Golgi-processed forms of Pmel17 that have been proteolytically processed in endosomes. *J Biol Chem* 283(4):2307–2322.
27. Hoashi T, et al. (2006) The repeat domain of the melanosomal matrix protein PMEL17/GP100 is required for the formation of organellar fibers. *J Biol Chem* 281(30):21198–21208.
28. Fredriksson S, et al. (2002) Protein detection using proximity-dependent DNA ligation assays. *Nat Biotechnol* 20(5):473–477.
29. Ahmed RR, et al. (2010) BACE1 and BACE2 enzymatic activities in Alzheimer's disease. *J Neurochem* 112(4):1045–1053.
30. Sun X, He G, Song W (2006) BACE2, as a novel APP theta-secretase, is not responsible for the pathogenesis of Alzheimer's disease in Down syndrome. *FASEB J* 20(9):1369–1376.
31. Abdul-Hay SO, Sahara T, McBride M, Kang D, Leissring MA (2012) Identification of BACE2 as an avid ß-amyloid-degrading protease. *Mol Neurodegener* 7:46.
32. Esterházy D, et al. (2011) Bace2 is a β cell-enriched protease that regulates pancreatic β cell function and mass. *Cell Metab* 14(3):365–377.
33. van Bebber F, Hruscha A, Willem M, Schmid B, Haass C (2013) Loss of Bace2 in zebrafish affects melanocyte migration and is distinct from Bace1 knock out phenotypes. *J Neurochem*, 10.1111/jnc.12198.
34. Quevedo WC, Jr., Fleischmann RD (1980) Developmental biology of mammalian melanocytes. *J Invest Dermatol* 75(1):116–120.
35. Stutzer I, et al. (2013) Systematic proteomic analysis identifies beta-site amyloid precursor protein cleaving enzyme 2 and 1 (BACE2 and BACE1) substrates in pancreatic beta-cells. *J Biol Chem* 288(15):10536–10547.
36. Leonhardt RM, Vigneron N, Rahner C, Cresswell P (2011) Proprotein convertases process Pmel17 during secretion. *J Biol Chem* 286(11):9321–9337.
37. Dornier E, et al. (2012) TspanC8 tetraspanins regulate ADAM10/Kuzbanian trafficking and promote Notch activation in flies and mammals. *J Cell Biol* 199(3):481–496.
38. Rose AA, et al. (2010) ADAM10 releases a soluble form of the GPNMB/Osteoactivin extracellular domain with angiogenic properties. *PLoS ONE* 5(8):e12093.
39. Bennett DC, Lamoreux ML (2003) The color loci of mice–a genetic century. *Pigment Cell Res* 16(4):333–344.
40. Kuhn PH, et al. (2007) Regulated intramembrane proteolysis of the interleukin-1 receptor II by alpha-, beta-, and gamma-secretase. *J Biol Chem* 282(16):11982–11995.
41. Delevoye C, et al. (2009) AP-1 and KIF13A coordinate endosomal sorting and positioning during melanosome biogenesis. *J Cell Biol* 187(2):247–264.
42. Kremer JR, Mastronarde DN, McIntosh JR (1996) Computer visualization of three-dimensional image data using IMOD. *J Struct Biol* 116(1):71–76.
43. Seiji M, Fitzpatrick TB, Simpson RT, Birbeck MS (1963) Chemical composition and terminology of specialized organelles (melanosomes and melanin granules) in mammalian melanocytes. *Nature* 197:1082–1084.